Performance and limitations of using ELT and MCAO for 50 μas astrometry

Gabriele Rodeghiero,[a,b,c,*] Carmelo Arcidiacono,[d] Jörg-Uwe Pott,[a] Saavidra Perera,[a,e] Giorgio Pariani,[f] Demetrio Magrin,[d] Hannes Riechert,[a] Martin Glück,[a] Eric Gendron,[g] Davide Massari,[b] Jonas Sauter,[a] Maximilian Fabricius,[h] Maximilian Häberle,[a] Sebastian Meßlinger,[a] Ric Davies,[h] Paolo Ciliegi,[b] Matteo Lombini,[b] and Laura Schreiber[b]

[a]Max-Planck-Institut für Astronomie, Heidelberg, Germany
[b]INAF OAS, Bologna, Italy
[c]INAF Osservatorio Astronomico d'Abruzzo, Teramo, Italy
[d]INAF Osservatorio Astronomico di Padova, Padova, Italy
[e]Center for Astrophysics and Space Sciences, California United States
[f]INAF OA-Brera, Merate, Lc, Italy
[g]Université Paris Diderot, LESIA, Observatoire de Paris, CNRS, UPMC, Meudon, France
[h]Max Planck Institute for Extraterrestrial Physics, Garching Germany

Abstract. Multi-conjugated adaptive optics (MCAO) is essential for performing astrometry with the Extremely Large Telescope (ELT). Unlike most of the 8-m class telescopes, the ELT will be a fully adaptive telescope, and a significant portion of the adaptive optics (AO) dynamic range will be depleted by the correction and stabilization of the telescope aberrations and instabilities. MCAO systems are of particular interest for ground-based astrometry since they stabilize the low-order field distortions and transient plate scale instabilities, which originate from the telescope and in the instrument. All instruments have several optical elements relatively far away from the pupil that can potentially challenge the astrometric precision of the observations with their residual mid-spatial frequencies errors. Using a combined simulation of ray tracing and AO numerical codes, we assess the impact of these systematic errors at different field-of-view (FoV) scales and fitting scenarios. The distortions have been assessed at different sky position angles (PA) and indicate that over large FoVs only small PA ranges (± 1 deg to 3 deg) are accessible with astrometric residuals $\lesssim 50$ μas. A full compliance with the astrometric requirement, at any PA, is achievable for 2 arc sec^2 FoV patches already with a third-order polynomial. The natural partition of the optical system into three segments, i.e., the ELT, the MAORY MCAO module, and the MICADO instrument, resembles a splitting of the astrometric problem into the three subsystems that are characterized by different distortion amplitudes and calibration strategies. The result is a family portrait of the different optical segments with their specifications, dynamic motions, conjugation height, and AO correctability, leading to tracing their role in the bigger puzzle of the 50-μas as astrometric endeavor. [DOI: 10.1117/1.JATIS.7.3.035005]

Keywords: distortion; astrometry; mid-spatial frequencies; multi-conjugated adaptive optics.

Paper 21007AS received Jan. 14, 2021; accepted for publication Jul. 15, 2021; published online Aug. 9, 2021.

1 Introduction

Astrometry is a technically demanding observation mode similar to optical interferometry. Building on the legacy of astrometric space-based missions, such as Hipparcos,[1] Gaia,[2] and Hubble Space Telescope (HST),[3,4] which have revolutionized the measurement of stellar position, proper motion, and distance, now the new generation of extremely large telescopes, the

*Address all correspondence to Gabriele Rodeghiero, gabriele.rodeghiero@inaf.it

Extremely Large Telescope (ELT),[5] the Thirty Meter Telescope,[6] and the Giant Magellan Telescope,[7] will push the scientific application of relative astrometry from the ground. The ELT will provide extreme sensitivity and diffraction-limited performances, which drive the achievable astrometric precision, over fields arc min scale. The unprecedented depth and resolution of ELT's astrometric observations will enable the investigation of science cases of paramount importance for astronomy, such as the galactic super-massive black hole,[8] the intermediate-mass black holes in globular clusters,[9] or the properties of dark matter in dwarf galaxies.[10,11] Although the ELT is designed and built with the requirement to reach the diffraction limit, its first light instrument MICADO is designed to deliver images of astrometric quality at least in the H and K bands where the first generation adaptive optics (AO) systems will deliver the best Strehls (up to 70% in SCAO mode in K band). MAORY is the star-oriented Multi-conjugated adaptive optics (MCAO) system for the ELT and it is equipped with one or two postfocal deformable mirrors (PFDMs), three natural guide stars (NGS), and six laser guide stars (LGS) for the wavefront sensing and the tomographic reconstruction.[12] The relay provides a one-to-one image of the ELT focal plane at an accessible position for MICADO and a second future instrument. MICADO's top-level requirement is to achieve star-to-star relative distance measurements to an accuracy of at least 50 μas over the central 20 arc sec field of view (FoV). Although the design of the instrument contributes to this requirement by a combination of low-distortion optical design and optomechanical stability (hence calibrateability), the best relative astrometric performance in the range of 20 to 50 μas will only be achieved in fields that provide a sufficient number of well-measured stars. This constraint is typically fulfilled for galactic targets and some extragalactic targets nearby (see discussion in Ref. 13) and is well known from previous relative astrometric mission, both space- and ground-based. In particular, large ground-based astrometry relies on low-order astrometric (plate-scale) calibration via reference stars since atmospheric refraction and telescope alignment are never perfectly stable at the required precision levels. Typically, the astrometric requirement is more than 100 times smaller than the diffraction limit, which renders any effort to actively control the astrometric stability in real-time very difficult. Since technically an astrometric distance measurement is equivalent to calibrating and knowing the plate-scale of the image, the astrometric precision is best expressed as relative precision, i.e., 50 μas precision/5 arc sec distances. This 10^{-5} level is the central astrometric requirement of the MICADO development for arcsec scale star-to-star distances and is derived from astrometric science cases such as kinematic estimation of the central dark mass in star clusters and nuclei of nearby galaxies. There is no perfect machine to perform astrometry. On the one hand, space telescopes profit from an extremely stable environment where to operate, their collecting area is limited. However, on the other hand, the large apertures of the next generation of ELTs will boost the sensitivity of the observations ($\sim D^3$) and the astrometric precision ($\sigma \sim \frac{\mathrm{FWHM}}{\mathrm{SNR}}$), but they will be continuously immersed in a changing, perturbing environment. Some of the perturbations affect the telescope with a variable but repeatable amplitude such as gravity, whereas some others such as the wind and temperature influence the system in a random way. The size of future instruments requires their installation at the Nasmyth platform in a gravity invariant configuration that maximizes their optomechanical stability. Using the system ELT-MAORY-MICADO as a representative test-bench of the ELTs astrometric instruments generation, the optomechanics follows a thread of increasing stability moving from the telescope (class 40 m) to the MCAO module (class 8 m) and the instrument (class 3 m). The telescope-born distortions are characterized by low-order terms; the warm MAORY optics have larger distortions (with respect to the ELT) but higher optomechanical stability, whereas the cold MICADO optics have even higher distortions due to the magnifying optics, but extreme stability. For instruments such as MICADO[14] and IRIS,[15] the common figure of merit for the relative astrometry at single- and multi-epoch observations is 50 μas in the near-infrared (NIR) for sources $\sim$1 as apart. The origin and fundamental limits of achieving 50 μas-level astrometry with the ELT/MICADO was discussed by Pott et al.[16] Generally, NIR refers to a wavelength range of 0.8 to 2.4 μm where typically higher AO performances (and boosted astrometry) are achieved at the red side of this range (H-K band). The $\simeq$50 μas precision is intended as postfit, differential astrometry after having applied third to fifth or higher order polynomials that fit and remove the distortion pattern induced by the instrument to the image. Among the different polynomial bases, the commonly used are the Cartesian[13] and Chebyshev[17] polynomials. The current astrometric noise floor for

instruments as NIRC2 at Keck and WFC3 on HST is ∼0.15 mas;[18] GeMS, a Cassegrain-focus, MCAO assisted instrument, shows residuals errors at ∼0.4 mas[17,19] that could be due to a variable gravity torque of the instrument at the telescope. MICADO is targeted to be the synthesis of the best characteristics of the previous astrometric imagers in terms of optomechanical stability located at the Nasmyth focus and the sensitivity gain from the ELT. Although the instrument design is astrometry oriented[14] and it provides an imaging channel with no moving parts to ensure the highest stability, several systematics notch the astrometric precision at different levels. The astrometric error budget takes into account the nominal distortion by design, the as-built manufacturing residuals, the tolerances, and the AO corrections. Particular attention should be paid to understanding the distortion effects due to the mid-spatial frequencies (MSF) coming from the manufacturing residuals and the quasistatic aberrations that can be partially absorbed by the deformable mirrors (DMs) of the MCAO system. In this paper, we investigate the limit to the aberrations correctability due to the wavefront sensing sampling, the DMs finite number of actuators, and the different conjugation heights of the optics with respect to the atmospheric turbulence layers in which the DMs are conjugated. Excluding the astronomical-borne errors discussed by Trippe,[20] the telescope and instrument-based errors constitute a significant fraction of the astrometric error budget analyzed in this work. A detailed analytical work by Ellerbroek[21] has proposed a Fourier domain approach, in which the errors on the optical surfaces are modeled as phase screens with stationary statistics at one or several conjugate ranges from the optical system pupil. The work considers three classes of errors affecting the astrometric observations, namely the quasistatic surface errors, which change between observations; the so-called beam wander errors that make the beamprint move onto the optics; and the calibration and under-sampling errors. The current work assesses the same classes of errors as Ellebroek[21] with a numerical approach based on a combination of a ray tracing model (Zemax) and a numerical AO simulator (MAO[22]). Although the analytical treatment provides a generalized approach applicable to any optical system, our numerical analysis specifically applies to the system ELT + MAORY + MICADO. However, the current analysis digs deeper into the manufacturing residual patterns leading to the mid-spatial frequency errors (MSFE) and carries out an end-to-end simulation of the AO loop in response to them. This paper deals with the astrometric errors generated inside the ELT and MAORY. It does not cover the MICADO contributions that belong to the non-common-path-aberrations (NCPAs) and are therefore not correctable by the AO system. This paper starts with the introduction of the concepts of conjugation height and optics correctability (Sec. 2). While dealing with the instrumental errors, particular care is given to the description of the quasistatic low-order aberrations and plate scale (PS) drifts (Sec. 3) and the MSF as it is a major challenge to the astrometric observations (Sec. 4). Section 5 describes the workflow and the methodology used for a simplified case study for the ELT and its MCAO system. The results are presented in Sec. 6.

2 Concept of Conjugation Height: Optics Correctability

A key concept to understanding how much a certain distortion factor can affect the astrometry is the conjugation height. The quantity can be seen as the optical distance from the instrument focal plane and its pupil. Every systematic error happening at the pupil plane applies equally to every field point in the FoV of the instrument, and therefore it is not critical for the relative astrometry. Conversely, every perturbation taking place close to the focal plane applies differentially among the field points and creates an astrometric error. For AO instruments, the conjugation height matters also as the distance between a certain optical surface and the plane at which the DM is conjugated. In addition to the different natures and amplitudes of the instrumental errors, their dangerousness is directly proportional to the proximity with the focal plane (conjugation height) and to their conjugation distance from the DMs (correctability). Table 1 collects the conjugation heights of the ELT and MAORY optics.[23]

The ELT is composed of five mirrors, three with the optical power arranged in a three mirror anastigmat configuration, one DM (M4), and a flat tip-tilt mirror (M5). All of the optics are sufficiently far, in terms of conjugation height (see Table 1), from the focal plane and reasonably close to the pupil plane such that they do not present a particular challenge for the astrometry in relation to the differential distortions over the FoV. Unlike the telescope, a few MAORY optical

Table 1 Conjugation heights of the ELT and MAORY optics. The footprint percentage represents the fraction of the optical surface covered by the light beam on the optics. Although the conjugation height of the ELT optics is relatively close to the conjugation of M4, the MAORY optics spreads over a wide range of values mostly farther away from the DMs heights. The MAORY optics nomenclature follows the progressive enumeration of the ELT optics.

DMs	Conj h (km)	Actuators
M4	0.625	5316
Postfocal DM	15.4	784
M5 TT mirror	−3.31	—
ELT	Conj h (km)	Footprint (%)
M2	−0.304	99.3
M3	3.54	93.4
M4 (DM)	0.625	98.7
M5	−3.31	94.9
MAORY		
M6	95.86	18.2
M7	34.38	14
M8 (DM)	15.40	76.5
M9	5.22	89.7
Dichroic	−6.64	87.9
M10	−26.5	25.6
M11	−207.5	19.8

elements are conjugated to heights far away from the pupil and close to the instrument focal plane, thus threatening the astrometric precision. By design, the PFDMs of an MCAO system are conjugated at specific altitudes where a permanent atmospheric turbulence layer lies.[24] One DM, close to the pupil, is conjugated at the ground layer where the largest turbulence concentrates, and one (or more) DMs are conjugated at higher atmospheric layers to improve the correction over a wider FoV. The ELT-M1 is the entrance pupil of the system, so it does not contribute to any differential astrometric error since all field points see the same aberrations and distortions. The other optical elements of the telescope and the instrument are generally conjugated at different, often random, altitudes since their position follows other design and performance optimizations. As a result, many aberrations on the optical elements of the system are potentially misconjugated with respect to the DMs and therefore have a limited correction power on them. To evaluate the correction capabilities of the DM conjugation plane, i.e., ELT-M4 and one postfocal DM at 15 km (M8), end-to-end simulations using SOAPY were performed. Soapy is a Python Monte-Carlo AO simulation toolkit.[25] The simulation parameters included the two DMs, three NGS, and six LGS. The DMs had 67×67 actuators (M4, 4489 active) and 28×28 actuators (M8, 784 active), respectively. Figure 1 shows how the long exposure Strehl ratio changes by assuming a single-layer turbulent profile of $r_0 = 0.16$ m at various altitudes. The turbulence layer is placed alternately at the conjugation height of the system optics to assess the ability of the MCAO compensation at the specific height of that optical element. As expected and asforeseen by Ragazzoni et al.,[26] there are two peaks where the altitude of the single turbulent layer is the same as the DM conjugation altitudes. This means that the wavefront error (WFE) can be properly corrected only around the DM altitudes and the correction quickly

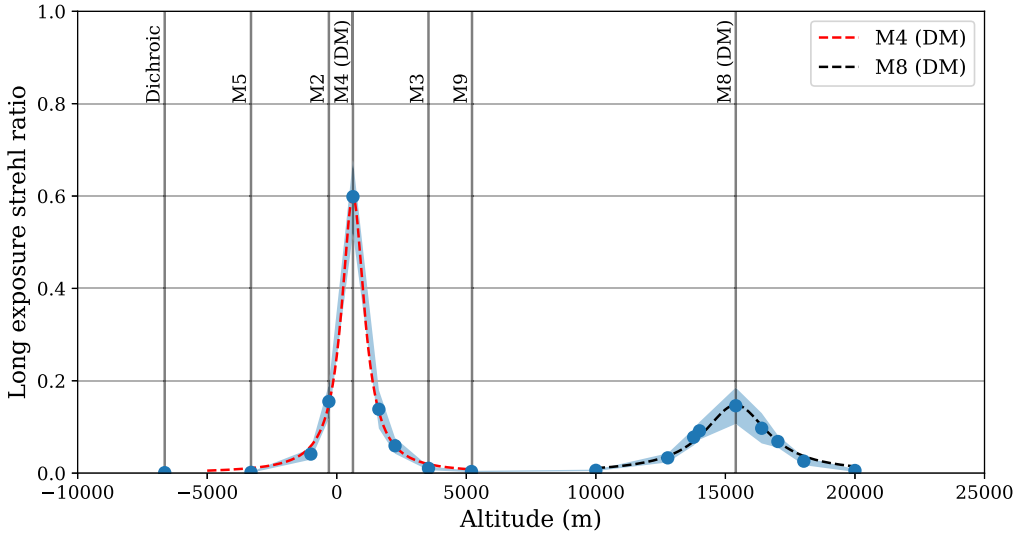

Fig. 1 Simulation showing the Strehl ratio achieved in the presence of a single turbulent layer over a range of altitudes (blue points). The dashed lines illustrate a Lorentzian fit of the two peaks centered at altitudes of M4 (red) and M8 (black). The gray lines indicate the locations of the ELT and MAORY mirrors within this altitude range. The optics with extreme conjugation heights fall outside the plot scale.

degrades following a hyperbolic profile as the misconjugation altitude among the perturbing element and the DM increases. However, the spread of these peaks differs, with the FWHM of ELT-M4 and M8 equating to 1261 and 3577 m, respectively. In this simulation, the turbulent layer is used as a proxy for the optics aberrations and MSF to infer the extent of the DM correction range.

As can be observed in Fig. 1, some of the ELT mirrors fall in the correction range of the ELT-M4, whereas the MAORY optics fall outside the range of both DMs. The optics with extreme conjugation heights are not shown since they exceed the plot scale. The misconjugation between the DMs and the other optics is doubly challenging. On the one hand, the aberrations of the surfaces are seen by the wavefront sensor (WFS), but they can be compensated for (to a certain extent) only if the optics is nearby in terms of conjugation to the DM. On the other hand, if aberrations are measured with the WFS and uploaded to the real-time computer (RTC) but the DM cannot reach the surfaces to be corrected, the AO system might inject systematic errors. The suppression of an aberration at a certain spatial scale depends also on its visibility at the WFS in terms of wavefront sampling and on the number of available modes of the DM.

3 Low-Order Distortions and Plate Scale Drifts

After introducing the optical conjugation problem, we survey the main instrument-born errors that affect the MICADO astrometry at the ELT. Table 2 lists the main astrometric error contributions of the ELT and MAORY system with their typical order of distortion, timescale of change, deterministic or random nature, and potential correctability. The different items in this table are discussed in the text following their listing order. We recall that the DM embedded in the ELT is M4, whereas the PFDMs are the DMs inside the MAORY relay.

Although the ELT optics do not introduce significant differential field distortions, the opto-mechanical instabilities of the system due to the environmental drifts and pointing/tracking motions can impact the precision of the astrometric observations and require the AO intervention to contain the negative effects. Differently from the current 8-m class telescopes, with the next generation of the ELTs, a significant fraction of the AO correction range is reserved for the suppression of the telescope-born aberrations. Previous work on this topic[13] underlined the importance of the MCAO stabilization for the astrometric observations against wind and gravity-induced PS and low-order aberrations of the telescope (Table 2). A Monte Carlo analysis of

Table 2 Main instrumental sources of error for the MICADO astrometry. Different contributions are listed together with their impacts in terms of polynomial order of the distortion generated, time-scale of variation and nature [(R)andom or (D)eterministic], and their potential damping with the active and AO of the ELT and MAORY.

Error contributions to astrometry	Type of distortion	Time-scale variation	Deterministic-random	Compensatable
ELT gravity flexure	PS and third	Minutes to hour	D	Yes with M4, PFDMs, and ROUS
ELT wind perturbations	PS and third	Sub-, second	R	Yes with M4 and PFDMs
ELT temperature drift	PS and third	Hours	R/D	Yes with M4, PFDMs, and ROUS
ELT optics manufacturing and print-through	PS and third	—	D	Partially with M4
MAORY temperature drift	Up to fifth	Hours	R/D	Yes with M4 and PFDMs
Interface tolerances ELT-MAORY	Up to third	Hours	R/D	Yes with M4 and PFDMs
MAORY optics alignment drift	Up to fifth	Days	D	Partially with M4 and PFDMs
MAORY PFDMs atmospheric correction	Up to fifth	Subsecond	R	No
MAORY optics manufacturing and MSF	Up to ninth	—	D	No

the ELT optics positioning errors has shown that the telescope produces distortion variations up to $\sim \pm 6$ mas arcmin^{-1} during nominal operation scenarios. These distortions are dominated by PS and third-order terms that can easily be removed with a polynomial fit if 3 and 10 reference stars are, respectively, available in the field. The PS drift is mostly induced by the axial motion of the ELT-M2 scales as $\sigma_{PS} \sim 15$ μas mm^{-1} (ELT PS $\sim$0.3016 arc sec mm^{-1}). The optomechanical structure and stability of the ELT require a periodic recollimation of the powered optics every $\sim$5 min with the Recurrent Optimization of Units Stroke (ROUS) loop.[27] Given the timescales of occurrence and duration of the cycle, the ROUS can be regarded as an active optics action. At the end of the ROUS, the ELT optical configuration is restored together with the nominal PS. Depending on the perturbing element, the timescale of the drifts also changes. Gravity (Table 2) is driven by the pointing and tracking of the telescope, and it can be reasonably absorbed by active optics mechanisms and the ROUS. The wind instead acts on much faster timescales (subseconds) that can be damped only by the AO loop. The compensation for the PS and focus changes induced by focal length variations requires a minimum of two DMs: one to address the focus and the other to restore the PS. By definition, an SCAO system minimizes the phase error in the pupil and, therefore, is insensitive to PS drifts. Hence, to control the PS, an MCAO system is required. The temperature is another perturbing transient of the optomechanical structure of the telescope that for the timescales of change can be comparable with gravity and absorbable with the ROUS. The average thermal expansion of the telescope structure[27] ($dz \sim 0.36$ mm K^{-1}) translates to $\sim$5.4 μas K^{-1} astrometric error that is driven by the temperature gradient of the night and spans between tens of minutes to hours. In addition to the as-built manufacturing errors, large optics, of class 2 to 4 m such as those of the ELT,[28] suffer from quasistatic and slow time-variable aberrations caused by the gravity warping, wind pressure, thermal gradient print-through,[27,29] and manufacturing print-through errors. The latter originates from the displacement of unsupported optical surface portions of a light-weighted mirror during the polishing phase of the blank. These optics figure errors are predominantly low-order aberrations, they sum to the manufacturing residuals errors, and they can be partially compensated for by the AO system as shown in Sec. 6. However, the AO system induces certain effects on astrometry, specific to the

ELT. The M5 together with the M3 and M4 behaves similar to a k-mirror, and when it is actuated for the atmospheric tip-tilt jitter stabilization, it induces a field rotation. As a result, the point spread function (PSF) gets elongated, and the effect becomes more prominent toward the outskirts of the MICADO FoV. Since the tip-tilt jitter is essential to retrieving good astronomical observations, the astrometric imaging mode will suffer some field limitations. This effect is not simulated in this work since its amplitude and the limitations to astrometry were assessed in a previous work.[13] Moving downstream the ELT focal plane, we encounter the MAORY optics and enter the second half of Table 2. Although the optical design of MAORY has undergone several configuration changes over the past few years,[23,30] the validity of the following astrometric considerations described in this section applies to all of them. As mentioned above, an MCAO system is a key element not only for providing a good Strehl ratio over a wide FoV but also for stabilizing the PS drifts and low-order distortions.[13] As for the telescope, MAORY can compensate for the temperature drift and the internal misalignment of its optics using the MCAO loop. Also the optomechanical misalingments happening at the two system interfaces, ELT-MAORY and MAORY-MICADO, can produce defocus, PS, and pointing error that are efficiently removed by the MCAO loop. A study of the optomechanical stability of the MCAO module has been assessed by Patti et al.,[31] and in a subsequent work,[32] the same authors studied the impact of the optical manufacturing residuals aberrations on the astrometry. For both tolerance types, an astrometric error of $\sim$50 μas can be achieved for typical exposure times of $\sim$2 min using fifth-order polynomials. We remind that a minimum of (3, 10, and 21) reference stars is required for (first, third, and fifth) polynomial orders, respectively. The MICADO $\sim$50 μas astrometric requirement has been verified by simulation, and it also takes into account the variation of the distortion pattern at different field rotation positions.[32] In addition, the MAORY distortion on the NGS probes can also inject a spurious astrometric signal into the MICADO FoV. A rigid shift of the three NGS WFSs results in a drift of the field on MICADO, whereas a radial motion of the probes causes a PS change in the FoV.[33] Patti et al.[32] quantified at $\sim$0.5 mas (average value) the effect of tip-tilt and PS errors related to the NGS probe position variations. Higher order flexures have not been assessed yet and require finite-element analyses of the bench. When in close loop, the MCAO system performs kHz corrections of the DMs shapes to counteract the WFE due to the atmospheric turbulence. This action changes the optical power of the DMs, and specifically for the PFDMs, this happens in planes not conjugated to the pupil, thus creating possible systematic distortions. Although this aspect is not treated in this work since no atmospheric modeling is provided in the analysis, for a perfectly random atmospheric perturbation, the AO correction has zero average, and therefore it should not introduce significant errors over exposures of minutes timescales. The last item of Table 2, the optics manufacturing errors, represents the main contribution to the astrometric error budget made by MAORY. The MCAO module is placed at the Nasmyth platform and is not equipped with a derotator; the starlight consequently moves on top of its optics at a velocity depending on the elevation angle of the telescope. The length of the trail run across by the light beams depends on the duration of the exposure frame. During this rotation, the manufacturing errors, and especially the MSFE, have the largest impact on the image distortion. These types of errors produce high-order distortions (easily up to ninth order) that limit both the achievable astrometric precision and the correctable FoV for astrometry as discussed in Sec. 6. Downstream the MAORY optics, the field derotation is performed by MICADO (unique degree of freedom), which compensates for the sky sidereal motion and what is left is the geometric distortion that perturbs the PSF position. Within a single exposure, the relative derotation of MICADO with respect to MAORY gives origin to a variable geometric distortion pattern that translates to a PSF smearing that is a negligible fraction of its size (typically $\sim 1/10$). For a detailed discussion of the MSFE characteristics and effects on astrometry, see Secs. 4 and 6. MICADO is the last part of the optical train; it contains the scientific camera and is mounted in a gravity-invariant position underneath the last MAORY folding mirror into a cryogenic vessel. Differently from MAORY and the ELT, the whole MICADO instrument is part of the NCPAs, the WFE of which is not sensed by the MCAO WFS and therefore not compensated for. Any change, degradation, or distortion occurring into the cryostat is essentially uncorrectable by the AO system, posing important requirements on the derotation accuracy,[34] the optics stability and quality, and the rotation precision of the atmospheric dispersion compensator (ADC).[35] Since the AO correction

cannot reach this system, we do not analyze its distortions. Nevertheless, the distortion variations are expected to be very small since the imaging astrometric channel has no moving parts with the exception of the ADC, which is kept fixed during the exposure and can be calibrated out with a preobservation calibration[36] and with its optomechanics being immersed in a thermalized cryoenvironment.[37]

4 Mid-Spatial Frequency Challenge

Diffraction-limited optics also has surface manufacturing residual errors. The power spectrum of these residuals can be divided into three main classes: low order or figure errors, intermediary or waviness errors, and high-order surface roughness.[38] Differently from the low-order modes that can be represented by the first 10 to 15 Zernike terms[39] that carry most of the power spectrum content and affect mostly the diffraction-limited condition of the PSF, the MSF errors give rise to the optical distortions. The optical distortion by itself does not affect the PSF quality; rather it randomly shifts its position in the field, leading to a spurious astrometric signal. The surface roughness influences the stray and diffuse light of the PSF halo without threatening the astrometric information. The MSF can be conveniently described with a power law.[38,40] Following Hayden and Content,[41] an MSF map can be synthesized directly from its power spectral density (PSD) using a Lorentzian profile as given in the following equation:

$$\mathrm{PSD} = \frac{A}{(u^2 + v^2)^{\beta}}, \tag{1}$$

where A is the amplitude scaling factor ($\mathrm{nm}^2\,\mathrm{cm}^2$), β is the exponent of the power law that regulates the slope of the PSD, and u and v are the spatial frequencies (cm^{-1}) corresponding to the x and y directions, respectively. The MSF map is derived by the inverse Fourier transform of the PSD map. As reported in Fig. 2, different values of β retrieve different granularities of the MSF maps and therefore different distortions. The best approach to identify a tolerable, and manufacturing-feasible MSF profile, relies on directly assessing the level of distortions injected into the system by either simulating different PSD profiles or having some measured profiles provided by laboratories or companies.

Generally, the MSF errors have predominant features resonating with spatial frequencies comparable to the size of the manufacturing tool. In addition, by looking more in detail at the real manufactured optics, the MSF can have patterns such as raster, periodic features,[42] epicyclic,[43] or circular trails (see Fig. 3).

The presence of any periodic or regular residual pattern is potentially dangerous for the astrometric observations. Although a piece of optics has an invariant MSF pattern embedded onto it, the problems arise when the light beams reflected off the surface move on top of it as a result of the sidereal motion of the sky. In alt-azimuthal telescopes at the Nasmyth focus, the sky rotates onto the optics surfaces, and the beam footprints of the starlight propagating into the system move on the optics surfaces. As the light beams move, they cross different regions of the optical surface characterized by different MSF patterns, and they are affected by variable distortions

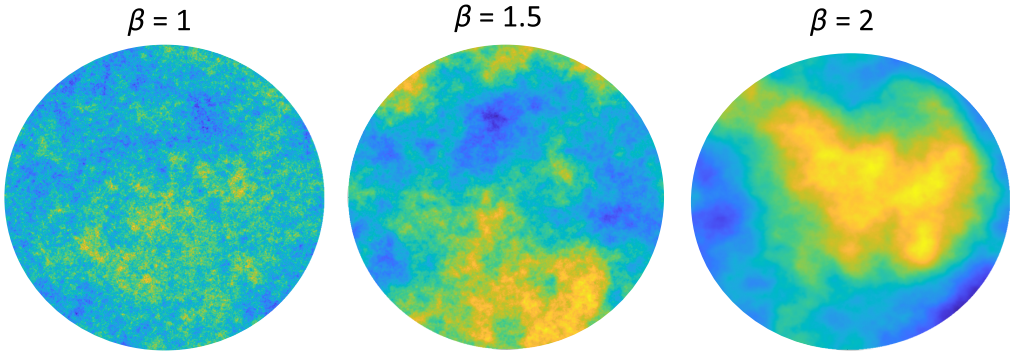

Fig. 2 MSF maps generated in MATLAB starting from PSD distributions with different β exponents.

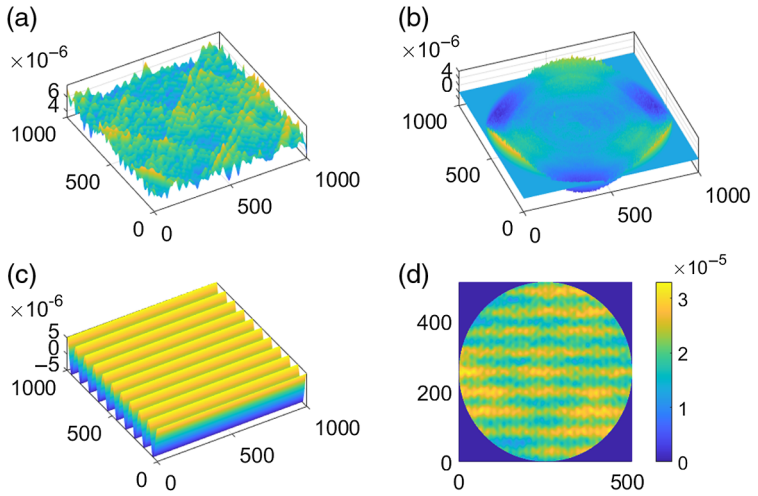

Fig. 3 MSF synthetic map (d) from the stack of three layers: epicyclic (a), concentric rings as measured on a real metal mirror (b), and raster (c). The unit of measurement of the map is mm.

over time. The complete suppression of the MSF patterns is technically impossible, and the best that can be done is trying repetitive passages of the polishing tool onto the surface in an epicyclic path[43] to cancel out most of the MSF power. As widely discussed in Sec. 2, the problem can be particularly nasty for the optics close to any focal plane in the system since the light beams from different fields are converging to focus and their footprints on the surface hit different, uncorrelated regions of the surface. As a result, different stars in the image see different and time-variant field distortions as the sidereal motion flows. Conversely, optics close to any pupil plane in the system has almost no impact on the relative astrometry because they apply the same distortion pattern to all field points (see Fig. 4).

The configuration where the MSF severely threatens the astrometry, boosting the distortions, takes place when the predominant (eventually periodic) pattern of the residuals is a fraction ($\sim 1/2$ to 1) of the beam footprint size. The impact on the distortion production depends also on the overlap of the beam footprint between adjacent fields of interest for astrometry ($\sim$1 as apart for MICADO). To underline this effect, a periodic pattern is applied to an optical surface located 350 mm away from the telescope focal plane, where the field light footprints have a diameter of 20 mm. The period and amplitude of the sinusoid are varied and rotated to simulate different position angles (PAs) on sky as shown in Fig. 5. The position of the centroids, 1 arc sec apart, is extracted at the MAORY exit focal plane and fitted with a fifth polynomial. The maximum distortion occurs for a sinusoid with a period that is twice the light footprint diameter.

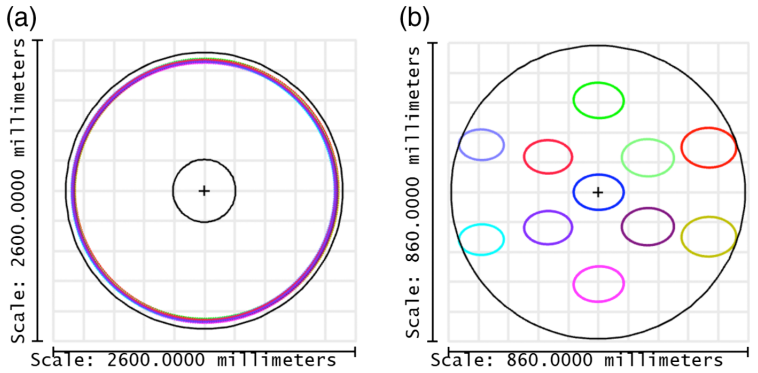

Fig. 4 (a) For optics close to the system pupil such as the ELT-M4, the light beam footprints from the different fields overlap and cover most of the surface, and they are affected by the same distortions. (b) The situation is the opposite for optics close to the instrument focal plane, where the light footprints hit non-overlapping surface patches with uncorrelated optical distortions.

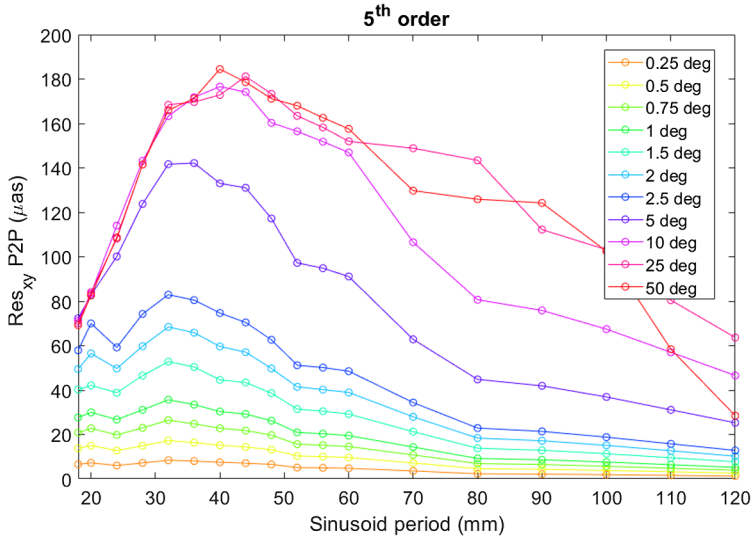

Fig. 5 Distortion errors show a trend with the pattern frequency with a maximum at twice the footprint dimension (40 mm), where two adjacent points on the plate see an opposite slope. The distortion increases almost linearly for small rotation angles, saturating above 5-deg rotation, where the effect of rotation is well randomized. Finally, in the high-frequency amplitude regime considered (10 to 40 nm PV), the distortion error residuals show a linear behavior.

In addition to the differential field distortions affecting the science FoV, the MSF inject spurious signals also in the AO WFS system. In an MCAO system such as MAORY, the wavefront sensing is performed using three NGS and six LGS with an asterism that maximizes the field coverage and requires a wide angular separation among the guide stars. In this way, the guide stars also suffer the same differential position jitter as their light beams move on the optical surfaces. This uncorrelated jitter triangulated among three guide stars can give origin to a fake PS signal in the WFS that is uploaded to the DM by the RTC and results in additional distortion of the science image.

5 Simulation Methodology

The simulation architecture embraces three different software tools: Zemax (now OpticStudio), MATLAB, and MAO (MAOR Adaptive Optics code). Although the former two are licensed software, the latter is a numerical simulation tool developed in an IDL environment for the AO modeling.[22] The workflow followed by the simulation is reported in Fig. 6 and listed as follows.

1. Generate MSF patterns (raster, periodic, and epicyclic) with MATLAB.
2. Import the MSF patterns in Zemax with grid sag surfaces, and project the same patterns in MAO at the optics conjugation heights and metapupils.
3. Observe the aberration with the MAO WFS, and close the loop to calculate the DMs response shapes.
4. Import the DMs shapes in MATLAB to fit a Zernike map onto them for the surface representation in Zemax.
5. Import the DMs Zernike maps in Zemax.
6. Export the geometric distortion maps at the instrument focal plane are from Zemax, and pass them to MATLAB.
7. Calculate the polynomial fit of the distortion patterns in MATLAB.

All of the steps involving Zemax and MATLAB are developed in a MATLAB environment using the ZOS-API functions that allow the direct communication and data/command exchange from MATLAB to Zemax.

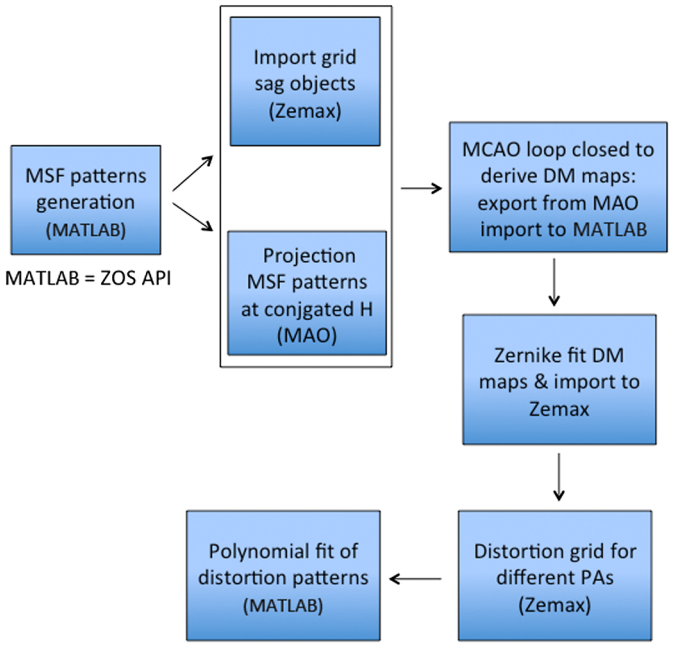

Fig. 6 Flowchart of the simulation architecture involving the three different softwares: MATLAB in a ZOS-API environment for direct link communication with Zemax and MAO developed in IDL language.

MAO is an IDL-based numerical tool developed specifically to support the simulation of the MAORY AO loop correction. In this analysis, we avoid introducing the atmospheric turbulence that is otherwise a common component of a simulation. Aiming to obtain high astrometric precision, we wish to disentangle it from the noise induced by the optical turbulence, focusing on the optical quality only. MAO is configured to use Zernike polynomials to produce a modal description of the MCAO (both M4 and one postfocal DM). MAO has no limitations on the order of the Zernike polynomials, whereas the representation of the MSF patterns in Zemax is performed using the grid sag surfaces. These surfaces are used to represent irregular sags when the basis such as the Zernike polynomials cannot fully represent the higher order spatial terms (Zemax is limited to the 231th Zernike term). A practical example of this limitation is shown in Fig. 7.

The sampling of the MSF patterns grid exported to MAO is tuned accordingly to the conjugation height of the optics that determines the linear size of the projected metapupil on sky:

$$D_{\mathrm{MP}} = 40\ \mathrm{m} + H_C \times \frac{\mathrm{FoV}}{206265''}, \tag{2}$$

where H_C is the conjugation height of the optic and 40 m refers to the diameter of the ELT entrance pupil. In Zemax, the grid sag surface shape is determined by a linear or bicubic spline interpolation of the sag discrete points and eventually their derivatives. Unfortunately, these types of surfaces are computationally heavy, and they might inject some additional distortion and PSF biases due to their discrete nature. The effect is visible as a pixelization of the PSF as shown in Fig. 8, and it occurs mostly when the grid sag surface is close to a pupil plane. It is therefore important to limit the use of these types of surfaces for optics far away from the pupil and to rely on Zernike surfaces whenever it is possible.

The scenario simulated in Zemax and MAO considers the ELT + MAORY and excludes MICADO. The latter has not been considered mainly because it belongs to the non-common path, so it is invisible to the WFSs and therefore uncorrectable. Since the presence of one or two PFDMs in MAORY is still under study in a trade-off between cost and performance, we assume conservatively for our study only one PFDM. The optics of MICADO is fixed, and the only variation of the distortion pattern is induced by the relative derotation between MICADO and MAORY that, in addition to the rotational errors, is repeatable and can be calibrated.

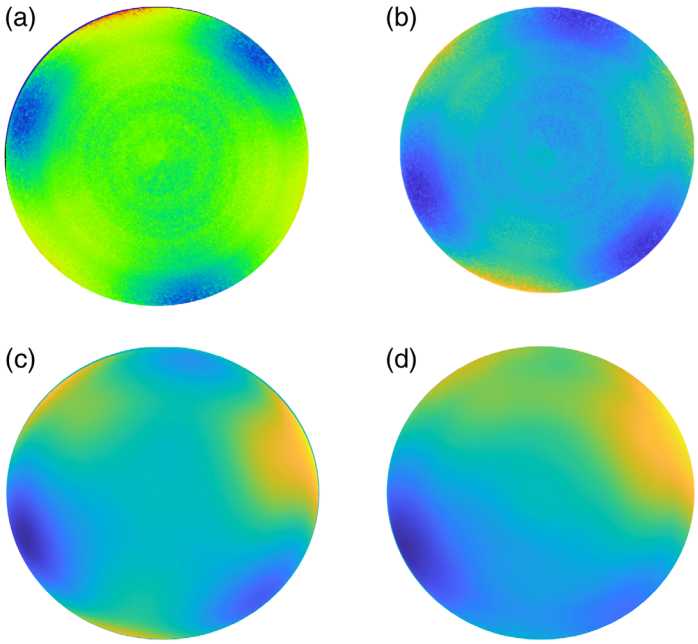

Fig. 7 Depending on the linear size of the optical surface to be simulated, the maximum number of Zernike terms (231) that can be simulated in Zemax can be sufficient (or not) to represent the MSF. In this case the measured map of a metal mirror (b) is well represented with a grid sag surface (a), whereas the Zernike maps with 37 (c) and 231 (d) do not adequately represent the surface texture, and with a higher number of terms the fit worsens.

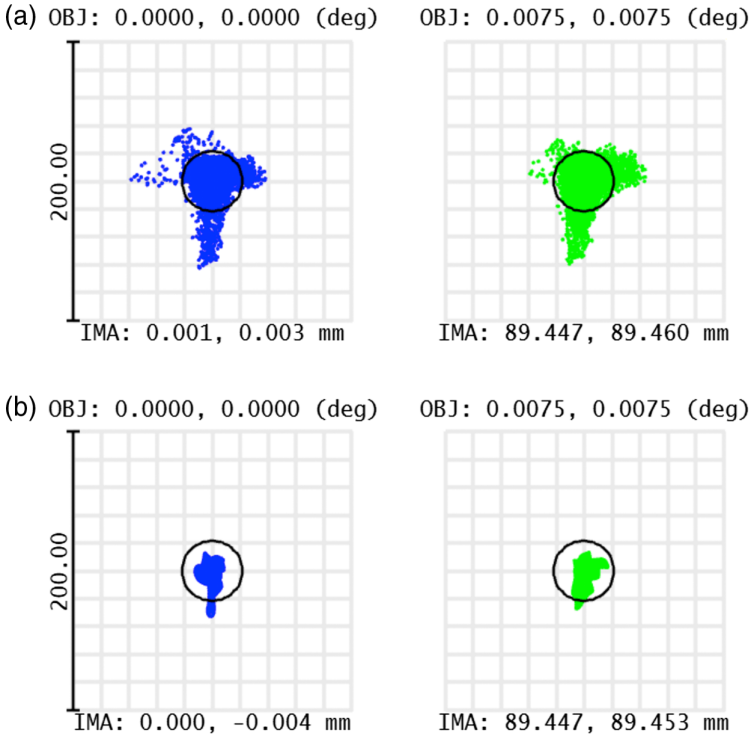

Fig. 8 (a) Pixelization effect of the PSF induced by the discrete number of points of the grid sag surface on the ELT-M2 that is relatively close to the system pupil. (b) The grid sag on the MAORY last folding mirror does not affect the morphology PSF when it is far away from the pupil. The black circle represents the Airy disk and the vertical bar illustrates the scale of the image in microns. The top and bottom numbers represent the angular and linear coordinates of the PSFs at the instrument focal plane, respectively.

In the optical design of the ELT + MAORY, we inserted MSF patterns synthesized in MATLAB on the ELT-M2, the MAORY dichroic, and the last folding mirror M11 using the methods described in Sec. 5. The optical specifications of the ELT-M2 allow for some low-order residuals of astigmatism and trefoil and about 40 nm root mean square (RMS) for the MSF.[28] Therefore, to the nominal sag of the M2, we added 100 nm of astigmatism (Z_6), 50 nm of trefoil (Z_{10}), and 25 nm peak to valley (PV) of epicyclic MSF pattern with a 4-mm pitch of the grid sag points. The expected print-through from gravity and temperature on the M2[27] has the same order of the abovementioned manufacturing residuals aberrations. To assess the impact of the gravity print-through on the M5, as a result of its three points support system,[44] we added a surface aberration of 100 nm RMS composed of vertical and oblique astigmatism and trefoil. On top of the dichroic and the M11, we added 5 to 10 nm PV of raster and epicyclic MSF patterns with a 0.74-mm pitch of the grid sag. The amplitude of the MSF aberrations has been tuned to typical manufacturing residuals for high-precision optics[43,45,46] and by checking that the impact on the PSF Strehl and PSF morphology. In parallel, the same aberrations have been projected as atmospheric phase screens at the conjugation altitude (Fig. 9) of the optics and the equivalent metapupils (Table 1) within the MAO simulator to retrieve the DMs shape response to them.

The analysis is limited to a scenario in which MAORY controls the MCAO loop with two DMs, M4 + one postfocal. To obtain a better interface with Zemax, we also opted for a fully illuminated circular ELT sized pupil. The MAORY NGS WFS and MICADO share the main MAORY optical train, with the NGS reaching larger angles that can be selected with a pick-off arm on a 160-arc sec FoV. The simulations take into account the different optical paths of the light beams that enter the WFSs in the MAORY patrol field and experience different spatial aberrations with respect to the science field. The simulations assume the system to be in optimal conditions for astrometry, i.e., available guide stars down to magnitude 17th in the H band that is the bright end of the NGS magnitude range. Interestingly, if the magnitude is 15th to 16th, the performance does not improve, whereas a scenario with one NGS with 17th and two NGSs with 19th is still acceptable. If the guide stars' asterism lies along one direction, the PS control suffers some anamorphism, and it can be stabilized only along the line drawn by the stars while the orthogonal component is mostly unconstrained. The laser part of the MAORY system is beyond the dichroic that splits the beam light into two: the visible part is redirected to the LGS WFS, whereas the NIR part is conveyed to MICADO. The LGS part may introduce NCPAs with respect to MICADO that are compensated for through calibrated look-up tables and a secondary WFS loop for truth sensing. MAORY's three Shack–Hartmann (SH) WFSs use the infrared part of the NGS light for fast tip-tilt and PS compensation (500 Hz), whereas the visible part is sent to the LGS high-order SH WFSs serving as reference for the NCPA component internal to MAORY

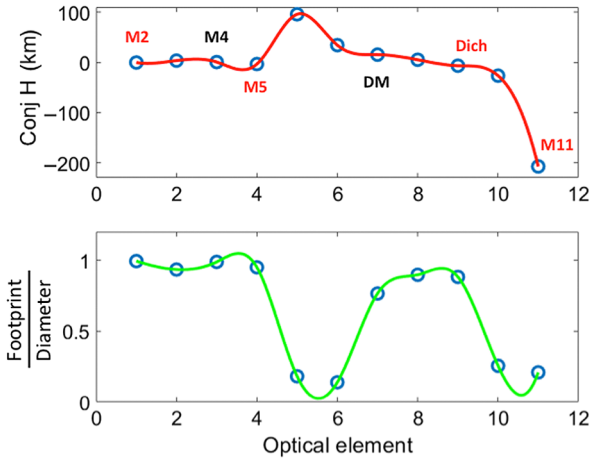

Fig. 9 The ELT and MAORY[23] optics have different conjugation heights that span between +95 and −200 km. The DMs conjugation heights are: ∼625 m for ELT-M4, ∼6 and ∼15 km for the MAORY postfocal DMs. The optics considered for the analysis of the MSF distortions, low-order aberrations, and print-through effects are highlighted in red; the DMs are in black.

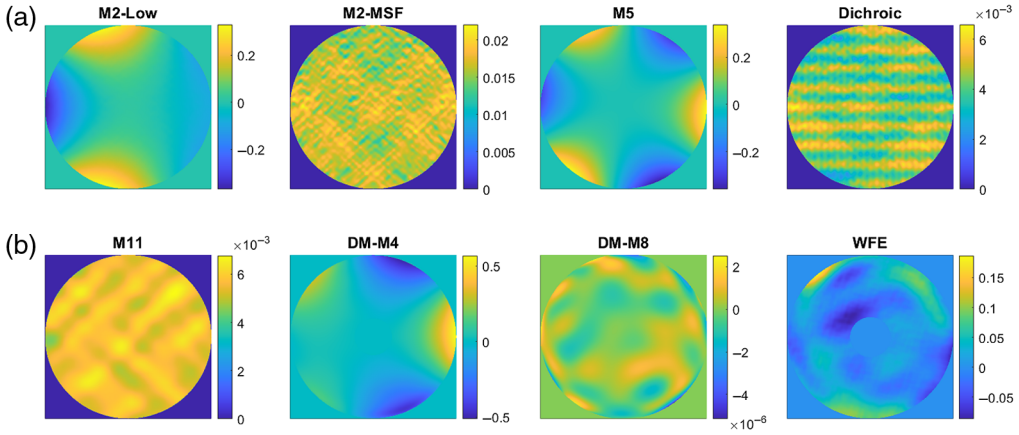

Fig. 10 (a) Overview of the surfaces with their low-order aberrations, print-through, and MSF patterns considered for the simulation. (b) DM shape response to the aberrations of the optics and MSF and final WFE at the system exit pupil. The unit of measure of the maps is microns.

system (LGS versus NGS). For this study, we configured MAORY such that all guide stars are represented as NGS. We accept the compromise of using a larger number (six + three) of NGS references while skipping the high-order correction controlled by the LGS WFS. Moreover, one of the worst offenders in terms of astrometric error are the MSF on top of the M11 that is unseen by the MAORY's LGS sensor. The truth sensing loop controls up to the MSF, since a 10×10 (or 20×20) lenslet arrays compose the SH sensor, whereas the high-order LGS is a 70×70. In the current simulation, 300 and 80 Zernike modes are controlled by the ground (M4) and high-layer conjugated DM, respectively. The AO response is uploaded to Zemax as a static DM shape once the AO loop has converged in the MAO simulation after a few hundreds of iterations. The DM shapes are represented with a Zernike basis up to the 231th in Zemax. An overview of the surface sag profiles of the simulated perturbed optics and the DMs response to them is shown in Fig. 10.

6 Results

In this section, we report the preliminary results of an exploratory study to assess the residual distortions in the presence of low-order aberrations and MSF for the ELT plus an MCAO system with one PFDM. Downstream all of the operations listed in Sec. 5, this overall simulation chain has been performed over different PAs to simulate observations at different epochs during the night. The optical distortion pattern is extracted using a Zemax macro that samples it with 961 equally spaced points over the MICADO FoV and fitted with a series of Cartesian polynomial orders in MATLAB. The astrometric postfit residuals for up to the ninth-order polynomial are shown over the full FoV (Fig. 11), for a FoV equivalent to 80% of a MICADO detector unit (Fig. 12), and over a 2-arc sec^2 patch FoV (Fig. 13). The results are presented using a boxplot graphic: the central red mark indicates the median, and the bottom and top edges of the blue box indicate the 25th and 75th percentiles, respectively. The whiskers extend to the most extreme data points, and the outliers are plotted individually using the "+" symbol. In the full FoV scenario, a single astrometric solution with residuals below 50 μas can be retrieved only for a PA range of ± 1 deg. Restricting to a fraction of 80% of a single MICADO detector, the PA range extends to ± 3 deg. When the fit is performed on a 2-arc sec^2 patch, the astrometric residuals are within the requirement for any PA for fit orders $\geq$3rd. For comparison, we show the distortion content of the nominal ELT + MAORY system with no MSFE in Fig. 14. The comparison with the distortion patterns affected by the MSFE is overwhelming and highlights the role of the worst offender for astrometry. Recalling that the minimum number of stars for a third-order polynomial is 10, this will limit the astrometric fields to dense stellar fields such as the globular cluster, the galactic center, and the dwarf galaxies. This constraint rules out, on average, the observability of the sparse galactic stellar fields that are intrinsically poor of objects. On the other hand, the sensitivity of the ELT will ensure the detection of a sufficient number of stars for the dense fields with a suitable SNR to perform 50 μas astrometry in the above-mentioned science cases.

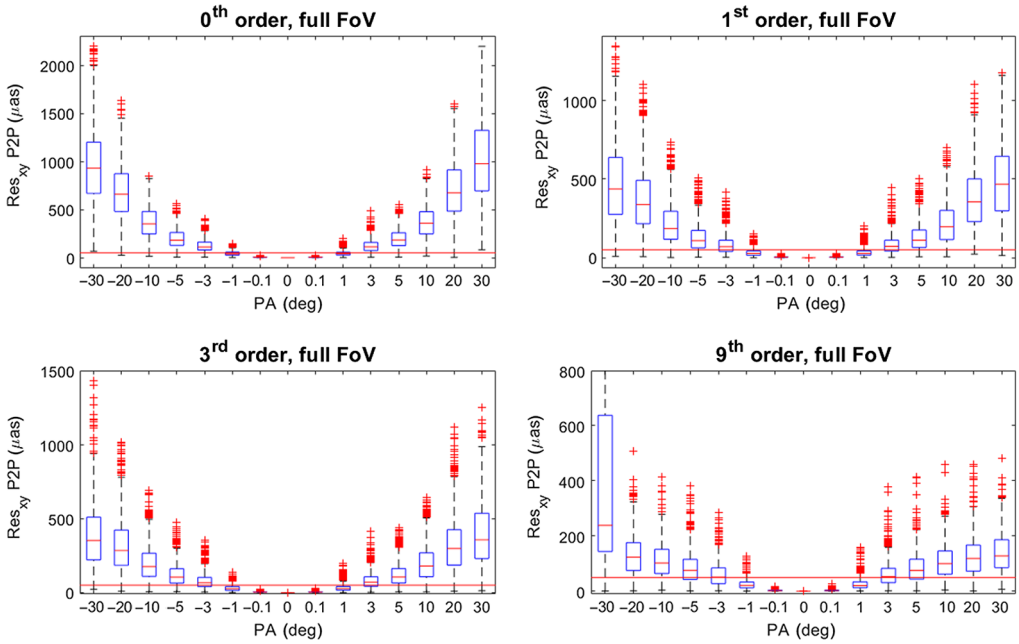

Fig. 11 Distribution of the point-to-point residual astrometric errors over the whole MICADO FoV for different PAs taking as reference frame the position at 0 deg for different fitting polynomial orders. The astrometric solution is fully compliant with the 50-μas requirement for a PA range restricted to ∼1 deg. Data are represented with boxplots: the central red mark indicates the median, and the bottom and top edges of the blue box indicate the 25th and 75th percentiles, respectively. The whiskers extend to the most extreme data points, and the outliers are plotted individually using the "+" symbol. The horizontal red line represents the MICADO astrometric requirement.

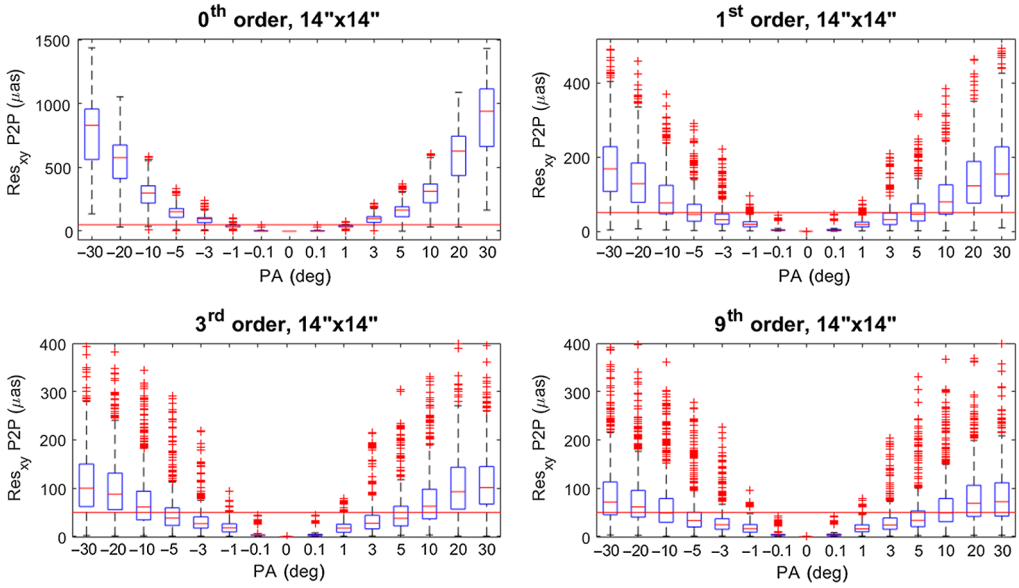

Fig. 12 The same analysis reported in Fig. 11 is reproposed here for a subset corresponding to the 80% of a MICADO detector unit. For each individual detector, we can retrieve astrometric residuals <50 μas within a PA range restricted to ∼3 deg.

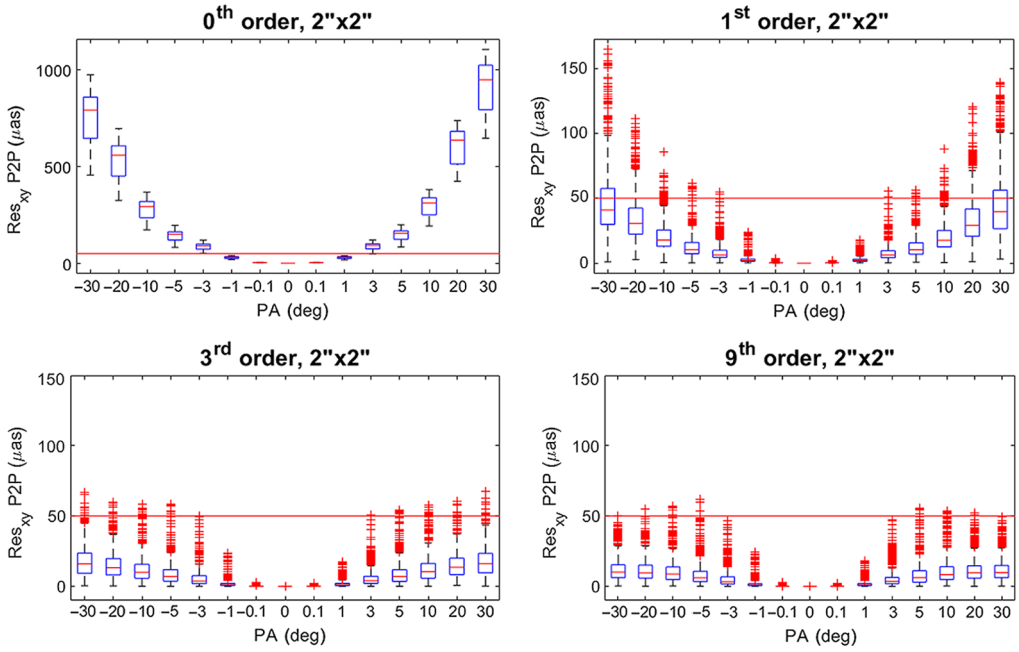

Fig. 13 The full compliance with the MICADO requirement is found for any PA if the polynomial fit is restricted to a 2-arcsec^2 FoV patch.

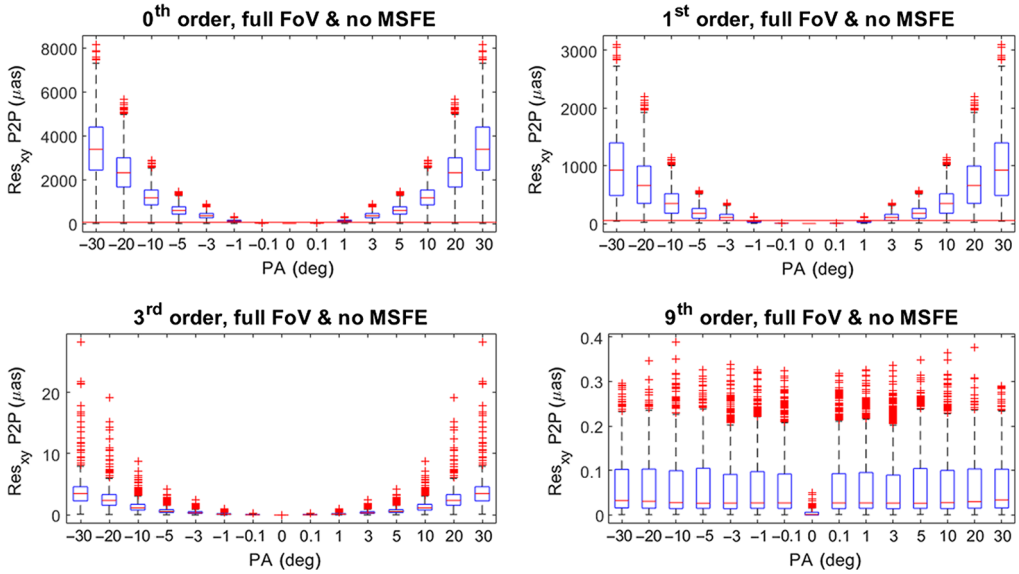

Fig. 14 When the MSFE is removed from the ELT and MAORY optics and only the nominal geometric distortion is left, the residual <50 μas for any PA over the full FoV already after a third polynomial is applied.

This distortion study concentrates on the distorted versus distorted (DD) frames at different PAs on sky without discussing the undistorted versus distorted frame (UD). The UD coordinates are the input (on-sky) field coordinates of the distortion sampling grid, and the DD coordinates are the output (at detector) field coordinates that are conjugated to the input UD. When comparing the DD coordinates, we look at the relative variation of two distortion patterns (i.e., relative astrometry) without gauging the absolute distortion content. Both coordinate comparisons matter and scale with each other because high absolute distortion leads to high sensitivity to the instabilities and therefore to large distortion variations. The DD frames allow us to explore the system's stability, whereas the UD leads to the absolute geometrical distortions. The former tells us

how quickly the distortions change and how often they need to be calibrated. The results obtained in this work tell us that a global, full FoV, astrometric solution is not possible, forcing the astrometric observations to work on smaller patches of the FoV. As for this work, previous experience with the MCAO system at GeMS[17,47] has shown that the astrometric solution built within a single detector is systematically better and preferable to the global solution over the full detector array. These simulations do not include stability effects of the optomechanical tolerances that have a similar impact on the size of the correctable FoV (1 to 2 arc sec) as stated by Pott et al.[16] The time-variant component of the distortions is represented here by the field rotation on top of the optics, which turns out to have a very similar amplitude and temporal behavior to the stability tolerances of the optics. The observation scenario shall be oriented toward the construction of local astrometric solutions over 2 arc sec^2 patches mosaicking larger fractions of the MICADO FoV or alternatively recalibrating the distortion pattern more frequently in the PA space when working on wider FoVs. MAORY and MICADO can be calibrated on sky at the expense of a large overhead on the observational time or using astrometric calibration masks[48] that are deployed at the entrance focal planes of the instruments to trace the optical distortions, and their variation, over the full FoV. The telescope has to be calibrated on sky, using stars as calibrators with absolute positions that are known at the time of the observations from Gaia and HST[47] and can be used up to $\sim$10 years from measurement. The limitations of the sky calibrations are described more extensively in other work.[13]

7 Conclusions

High-resolution imaging with MICADO at the ELT will lead to a significant leap forward in the astrometric observations for objects such as globular cluster, dwarf galaxies, and the galactic center. This work shows the impact that the MSF and low-order aberrations have on astrometry with the ELT and MAORY optics as well as their variation as seen at different PAs of the instrument. The optical ray tracing simulations from which the distortion patterns are retrieved include the DMs response to the MSF as calculated with the MAO simulator. The simulation indicates that the MSF and the low-order quasistatic aberrations of misconjugated optics to the DMs, by more than 3 to 5 km, remain essentially uncompensated for and give rise to variations of the distortion pattern as the light-beams move on top of the optical surfaces. The MSF and the low-order aberrations act on the production of high-order distortions and PS terms, respectively. A PS term can be compensated for with an MCAO system using two or more DMs to stabilize the field, while the high-order distortions (uncompensated for by AO) put a limit on the astrometric precision and the size of the observable FoV. The analysis underlines the impossibility of retrieving astrometric solutions over the full FoV and over the detector unit size for different PAs at the level of $\sim$50 μas. When working over large FoV fractions, only small PA ranges ($\pm$1 deg to 3 deg) are accessible with small astrometric residual errors. A full compliance, at any PA, with the MICADO astrometric requirement is achievable for 2 arc sec^2 FoV patches already with a third-order polynomial. The comparison with the nominal geometric distortion of the ELT and MAORY highlights that the MSFE is the worst offender for astrometry. The suitable tools for the mapping and calibration of the MSFE in MAORY and MICADO are the astrometric calibration masks while the telescope distortions should be calibrated on sky. This work is limited to a subsample of the ELT and MAORY optics, but the developed method and the simulation architecture can be extended to multiple optical surfaces and generalized to other instruments.

Acknowledgments

The authors were grateful to the anonymous referees for their comments that led to improvements in the manuscript and to Dr. Robert J. Harris for his useful suggestions and corrections.

References

1. M. Perryman, "EAS Tycho Brahe prize lecture 2011. Hipparcos: a retrospective," *Astron. Astrophys. Rev.* **19**, 45 (2011).

2. A. G. A. Brown et al., "Gaia data release 2," *Astron. Astrophys.* **616**, A1 (2018).
3. M. Libralato et al., "The HST large programme on ω Centauri. III. Absolute proper motion," *Astrophys. J.* **854**, 45 (2018).
4. A. Bellini, "Internal kinematics of globular clusters: current state of the art, issues, and what to expect from the future," *Proc. Int. Astron. Union* **14**(S351), 408–411 (2019).
5. R. Tamai et al., "The ESO's ELT construction status," *Proc. SPIE* **10700**, 1070014 (2018).
6. L. Simard, "The Thirty-Meter Telescope: science and instrumentation for a next-generation observatory," *J. Astrophys. Astron.* **34**, 97–120 (2013).
7. J. Fanson et al., "Overview and status of the Giant Magellan Telescope project," *Proc. SPIE* **10700**, 1070012 (2018).
8. Gravity Collaborationet al., "Detection of the gravitational redshift in the orbit of the star S2 near the Galactic centre massive black hole," *Astron. Astrophys.* **615**, L15 (2018).
9. J. Anderson and R. P. van der Marel, "New limits on an intermediate-mass black hole in Omega Centauri. I. Hubble space telescope photometry and proper motions," *Astrophys. J.* **710**, 1032–1062 (2010).
10. D. Massari et al., "Three-dimensional motions in the Sculptor dwarf galaxy as a glimpse of a new era," *Nat. Astron* **2**, 156–161 (2018).
11. D. Massari et al., "Stellar 3D kinematics in the Draco dwarf spheroidal galaxy," *Astron. Astrophys.* **633**, A36 (2020).
12. E. Diolaiti et al., "MAORY: adaptive optics module for the E-ELT," *Proc. SPIE* **9909**, 99092D (2016).
13. G. Rodeghiero et al., "The impact of ELT distortions and instabilities on future astrometric observations," *Mon. Not. R. Astron. Soc.* **479**, 1974–1985 (2018).
14. R. Davies et al., "The MICADO first light imager for the ELT: overview, operation, simulation," *Proc. SPIE* **10702**, 107021S (2018).
15. J. E. Larkin et al., "The infrared imaging spectrograph (IRIS) for TMT: instrument overview," *Proc. SPIE* **11447**, 114471Y (2020).
16. J. U. Pott et al., "The MICADO first light imager for ELT: its astrometric performance," *Proc. SPIE* **10702**, 1070290 (2018).
17. H. Riechert et al., "GeMS/GSAOI: towards regular astrometric distortion correction," *Proc. SPIE* **10702**, 1070232 (2018).
18. J. R. Lu et al., "Near-infrared astrometry of star clusters with different flavors of adaptive optics and HST," *Proc. SPIE* **9148**, 91480B (2014).
19. B. Neichel et al., "Astrometric performance of the Gemini multiconjugate adaptive optics system in crowded fields," *Mon. Not. R. Astron. Soc.* **445**, 500–514 (2014).
20. S. Trippe et al., "High-precision astrometry with MICADO at the European Extremely Large Telescope," *Mon. Not. R. Astron. Soc.* **402**, 1126–1140 (2010).
21. B. Ellerbroek, "A Fourier domain model for estimating astrometry errors due to static and quasi-static optical surface errors," *Astron. Astrophys.* **552**, A41 (2013).
22. C. Arcidiacono et al., "Numerical simulations of MAORY MCAO module for the ELT," *Proc. SPIE* **10703**, 107034I (2018).
23. M. Lombini, E. Diolaiti, and M. Patti, "Historic evolution of the optical design of the Multi Conjugate Adaptive Optics RelaY for the extremely large telescope," *Mon. Not. R. Astron. Soc.* **486**, 320–330 (2019).
24. F. J. Rigaut, B. L. Ellerbroek, and R. Flicker, "Principles, limitations, and performance of multiconjugate adaptive optics," *Proc. SPIE* **4007**, 1022–1031 (2000).
25. A. Reeves, "Soapy: an adaptive optics simulation written purely in python for rapid concept development," *Proc. SPIE* **9909**, 99097F (2016).
26. R. Ragazzoni et al., "Multiple field of view layer-oriented adaptive optics. Nearly whole sky coverage on 8 m class telescopes and beyond," *Astron. Astrophys.* **396**, 731–744 (2002).
27. M. Mueller et al., "The secondary mirror concept for the European Extremely Large Telescope," *Proc. SPIE* **9145**, 91451I (2014).
28. R. Geyl et al., "First steps in ELT optics polishing," *Proc. SPIE* **10829**, 1082904 (2018).
29. H. Bonnet et al., "Adaptive optics at the ESO ELT," *Proc. SPIE* **10703**, 1070310 (2018).
30. D. Magrin et al., "MAORY: optical configuration and expected optical performances," *Proc. SPIE* **11448**, 1144834 (2020).

31. M. Patti et al., "MAORY optical design analysis and tolerances," *Proc. SPIE* **10690**, 106902C (2018).
32. M. Patti et al., "The impact of geometric distortions in multiconjugate adaptive optics astrometric observations with future extremely large telescopes," *Mon. Not. R. Astron. Soc.* **487**, 1140–1148 (2019).
33. M. Bonaglia et al., "Status of the preliminary design of the NGS WFS subsystem of MAORY," *Proc. SPIE* **10703**, 107034D (2018).
34. S. Barboza et al., "The MICADO first light imager for ELT: derotator design status and prototype results," *Proc. SPIE* **10702**, 107028T (2018).
35. J. A. van den Born and W. Jellema, "Quantification of the expected residual dispersion of the MICADO near-IR imaging instrument," *Mon. Not. R. Astron. Soc.* **496**, 4266–4275 (2020).
36. J. A. van den Born et al., "A Fourier optics approach to evaluate the astrometric performance of MICADO," *Proc. SPIE* **11450**, 114500V (2020).
37. J. Schubert et al., "The MICADO first light imager for ELT: cold optics instrument," *Proc. SPIE* **10702**, 107028W (2018).
38. V. V. Martynov and Y. Y. Platonov, "Surface roughness analysis of multilayer x-ray optics," *Proc. SPIE* **7077**, 707704 (2008).
39. R. J. Noll, "Zernike polynomials and atmospheric turbulence," *J. Opt. Soc. Am.* **66**, 207–211 (1976).
40. A. Duparré et al., "Surface characterization techniques for determining the root-mean-square roughness and power spectral densities of optical components," *Appl. Opt.* **41**, 154–171 (2002).
41. J. E. Hayden and D. A. Content, "PSD data analysis and algorithm development," *Proc. SPIE* **10316**, 93–103 (2007).
42. B. Zhong et al., "Modelling and simulation of mid-spatial-frequency error generation in CCOS," *J. Eur. Opt. Soc.-Rapid Publ.* **14**, 4 (2018).
43. C. Reynolds et al., "A novel hyper-crossing tool path generation algorithm for sub-aperture polishing," *Proc. SPIE* **10706**, 107060F (2018).
44. M. Cayrel, "E-ELT optomechanics: overview," *Proc. SPIE* **8444**, 84441X (2012).
45. G. Yu, H. Li, and D. Walker, "Removal of mid spatial-frequency features in mirror segments," *J. Eur. Opt. Soc.-Rapid Pub.* **6**, 11044 (2011).
46. C. Maloney, J. P. Lormeau, and P. Dumas, "Improving low, mid and high-spatial frequency errors on advanced aspherical and freeform optics with MRF," *Proc. SPIE* **10009**, 100090R (2016).
47. D. Massari et al., "Astrometry with MCAO: HST-GeMS proper motions in the globular cluster NGC 6681," *Astron. Astrophys.* **595**, L2 (2016).
48. G. Rodeghiero et al., "Development of the warm astrometric mask for MICADO astrometry calibration," *Publ. Astron. Soc. Pac.* **131**, 054503 (2019).

Gabriele Rodeghiero received his BS and MS degrees in astronomy from the University of Padova in 2008 and 2011, respectively, and his PhD in astronomy with a focus on instrumentation for ground-based gamma ray astrophysics in collaboration with the Italian National Institute for Astrophysics (INAF) in 2015. He was a postdoctoral researcher at the Max Planck Institute for Astronomy, Heidelberg, Germany, from 2015 to 2020 working at the development of the MICADO calibration unit and standalone relay optics for the SCAO early science phase in the context of ground-based high-resolution NIR instrumentation. He has been a staff researcher at the INAF Astrophysics and Space Observatory, Bologna, Italy, and INAF Observatory of Abruzzo since September 2020 supporting the manufacturing, assembly, integration, and testing of the MAORY instrument and its calibration unit.

Saavidra Perera is a postdoctoral researcher at the University of California San Diego, USA, working on building and testing the new pyramid wavefront sensor for the Gemini Planet Imager instrument upgrade. Her research background is in designing and developing atmospheric turbulence profiling instruments and correction techniques for astronomy.

Biographies of the other authors are not available.